Structure and magnetism in epitaxial $Fe_{1+x}VSb$ nanocomposite films

Estiaque H. Shourov,[1] Chenyu Zhang,[1] Paul M. Voyles,[1] and Jason K. Kawasaki[1,*]

[1] *Materials Science and Engineering, University of Wisconsin–Madison*

(Dated: March 29, 2022)

The combination of ferromagnetism and semiconducting behavior offers an avenue for realizing novel spintronics and spin-enhanced thermoelectrics. Here we demonstrate the synthesis of doped and nanocomposite half Heusler $Fe_{1+x}VSb$ films by molecular beam epitaxy. For dilute excess Fe ($x < 0.1$), we observe a decrease in the Hall electron concentration and no secondary phases in X-ray diffraction. Magnetotransport measurements suggest weak ferromagnetism that onsets at a temperature of $T_c \approx 5$K. For higher Fe content ($x > 0.1$), ferromagnetic Fe nanostructures precipitate from the semiconducting FeVSb matrix. The Fe/FeVSb interfaces are epitaxial, as observed by transmission electron microscopy and X-ray diffraction. Magnetotransport measurements suggest proximity-induced magnetism in the FeVSb from the Fe/FeVSb interfaces, or superparamagnetically coupled Fe-rich clusters, at an onset temperature of $T_c \approx 20$K.

I. INTRODUCTION

Incorporating magnetism and epitaxial interfaces in semiconducting half Heusler compounds is attractive for applications in spintronics and thermoelectric power conversion. While half-Heusler compounds with 18 valence electrons per formula unit are generally diamagnetic semiconductors [1, 2], slight deviations from stoichiometry can make these materials magnetic [3, 4]. This provides a route to make new dilute magnetic semiconductors for applications in spintronics [5, 6]. Half-Heusler compounds are also attractive thermoelectric materials due to their large thermoelectric power factors [7] and the ability to precipitate nanostructures to decrease the thermal conductivity [8]. New concepts based on magnon drag [9] and spin fluctuations [10] suggest that incorporating magnetism may further increase the thermopower.

Here we explore the structure and magnetism of epitaxial thin films with total composition $Fe_{1+x}VSb$, grown by molecular beam epitaxy (MBE) on MgO (001) substrates. FeVSb is a semiconducting, 18 valence electron half Heusler compound. For dilute x, excess Fe is expected to dope into the FeVSb lattice and make this compound ferromagnetic [11]. For larger x, epitaxial Fe nanostructures are expected to precipitate from FeVSb, since FeVSb and bcc Fe are thermodynamically stable in contact with one another (they are joined by a tie line in the Fe-V-Sb phase diagram [12]) and they share similar lattice parameters ($a_{FeVSb} = 5.82$ Å, $2a_{Fe,bcc} = 5.73$ Å).

We show that for $Fe_{1+x}VSb$ epitaxial films with $x < 0.1$, no secondary phases are observed by X-ray diffraction and the films have a ferromagnetic onset temperature of $T_c \approx 5$K, as determined by magnetotransport measurements. However, we are not able to precisely determine the solubility limit for Fe in FeVSb. For $x > 0.1$ we observe epitaxial Fe precipitates embedded within a FeVSb matrix. In these Fe:FeVSb nanocomposites we identify two sources of magnetism: the ferromagnetic Fe precipitates ($T_c \gg 300$K) and proximity-induced ferromagnetism in the FeVSb, from the Fe/FeVSb interfaces. Our work identifies Fe/FeVSb as a clean system for exploring magnetic doping, epitaxial nanostructuring, and magnetic proximity effects in thermoelectric and spintronic materials.

II. RESULTS AND DISCUSSION

$Fe_{1+x}VSb$ films with varying x were grown by molecular beam epitaxy (MBE) on MgO (001) substrates. Samples were grown leveraging a semi-adsorption controlled growth window in which the Sb stoichiometry is self-limiting [13], at a substrate temperature of 560°C. The Fe and V fluxes were measured *in situ* using a quartz crystal microbalance (QCM) immediately prior to sample growth. Absolute compositions were calibrated using Rutherford Backscattering Spectrometry (RBS) on separate samples. Further details on the growth process can be found elsewhere [13].

In Fig. 1, we investigate the structural evolution of the films as a function of excess Fe. In the reflection high energy electron diffraction patterns (RHEED, Fig. 1(a)), all films display a characteristic 2× streaky reconstructed surface indicative of smooth epitaxial films. The 2× reconstruction is attributed to Sb dimerization which is well-known for antimonide half-Heusler surfaces [14].

X-ray diffraction (XRD) confirms that the films are all epitaxial. In the wide angle $2\theta - \omega$ scan (Fig. 1(b)), only 00l-type FeVSb (half-Heusler) and Fe (bcc) reflections are observed. For $x < 0.1$, high resolution scans around the FeVSb 004 reflection detect only the FeVSb half Heusler phase (Fig. 1c). In this dilute regime, we expect the excess Fe to occupy the tetrahedral interstitial $(\frac{3}{4}, \frac{1}{4}, \frac{1}{4})$ sites in the FeVSb lattice [15] (Fig. 1d, white spheres). For $x < 0.1$, while we do not observe a Fe bcc 002 reflection, it is possible that some bcc Fe phase is present, below the detection limit of XRD. For $x \geq 0.14$, we observe a secondary peak at $2\theta = 64.5$ degrees, which we attribute to the 002 reflection of body centered cubic Fe. The secondary peak grows in intensity with increas-

* jkawasaki@wisc.edu

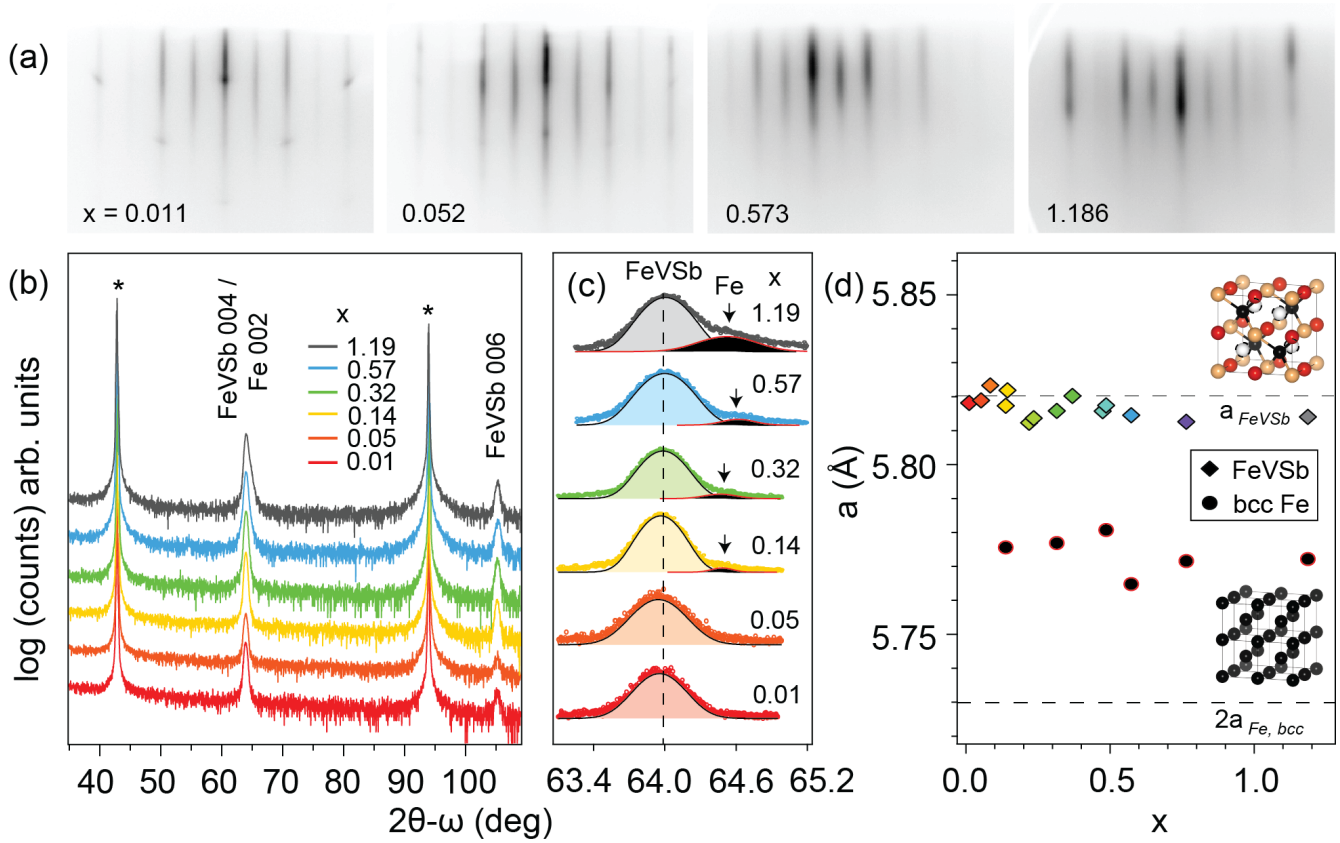

FIG. 1. **Structural evolution of epitaxial $Fe_{1+x}VSb$ films by electron and x-ray diffraction.** (a) RHEED pattern along the < 110 > azimuth, showing strong streaky 2× reconstruction over all compositions studied. (b) Wide angle XRD (Cu $K\alpha$) showing the half-Heusler 00l and Fe 002 reflections. Asterisks indicate the MgO substrate reflections. (c) High resolution scans of the FeVSb 004 reflections reveal the onset of a shoulder peak at composition $x = 0.14$, which we attribute to the 002 reflection of Fe (bcc). Shaded curves show the Gaussian fits. (d) Out of plane lattice parameter extracted from XRD as a function of excess Fe composition. Diamond and circle markers correspond to FeVSb and Fe respectively. Dotted lines show the lattice parameter of bulk FeVSb (half Heusler), and that of doubled body centered cubic Fe unit cells. Crystal structure models for FeVSb and Fe are shown. Black, red, orange and white spheres corresponds to Fe, V, Sb and interstitial respectively. For low x, excess Fe is expected to incorporate into the $(\frac{3}{4}, \frac{1}{4}, \frac{1}{4})$ tetrahedral interstitial sites of FeVSb (white spheres).

ing x, which we attribute to an increasing volume fraction of Fe precipitates. The lattice parameters (a) calculated from each peak are plotted in Fig. 1(d). The primary peak lattice parameter agrees well to that of bulk FeVSb. The secondary peak lattice parameter appears to match a dilated doubled unit cell of bcc Fe. We attribute the slight increase in lattice parameter of Fe to strain.

Scanning transmission electron microscopy (STEM) for samples with $x \geq 0.1$ confirms the existence of bcc Fe precipitates, embedded epitaxially within a FeVSb matrix. Fig. 2 shows a high angle annular dark field (HAADF) STEM image of a sample with $x = 0.46$, in which we identify a Fe precipitate. Closer analysis of the Fe/FeVSb interface reveals a cube on cube epitaxial relationship, with Fe(001)[110] ∥ FeVSb(001)[110]. We have identified Fe precipitates in $Fe_{1+x}VSb$ samples with x as small as 0.1 (supplement Fig. S-1). No Fe precipitates have been identified for samples with $x < 0.1$. Further structural analysis is required to more precisely determine the Fe solubility limit in FeVSb.

The dependence of the Hall mobility (μ) and carrier concentration (n_{3d}) on composition x provides an additional estimate of the solubility limit for excess Fe. Fig. 3 shows the mobility and carrier concentration extracted from Hall effect measurements. Since the samples with $x > 0$ are ferromagnetic and exhibit contributions from the anomalous Hall effect, we use a linear fit of $\rho_{xy}(B)$ at high field to extract the majority carrier concentration (Supplemental Fig. 3). We find that as a function of x, the electron concentration exhibits a minimum near $x \approx 0.05 - 0.1$ and the mobility exhibits a maximum near $x \approx 0.1 - 0.14$. These findings suggest that for low $x < 0.1$, the excess Fe acts to compensate free carriers in the FeVSb. Similar results have been observed experimentally for excess Ni in NiTiSn [16]. This implies that at low $x < 0.1$, the excess Fe may dope into the FeVSb lattice. First principles calculations suggest the most likely dopant site is the $(\frac{3}{4}, \frac{1}{4}, \frac{1}{4})$ vacancies in the

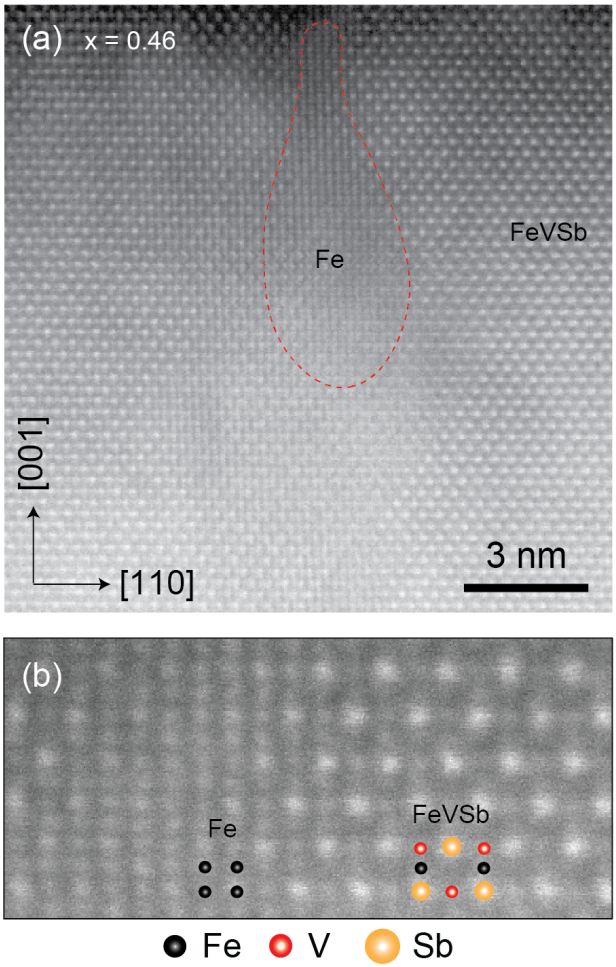

FIG. 2. **Cross-sectional STEM image showing Fe precipitation in the $Fe_{1.46}VSb$ film.** (a) HAADF-STEM image of nanometer scale Fe nanoprecipitates embedded in the FeVSb matrix. (b) High resolution image of Fe/FeVSb interface. Individual atoms are identified by atomic models, confirming the half-Heusler and *bcc* crystal structures of the two phases.

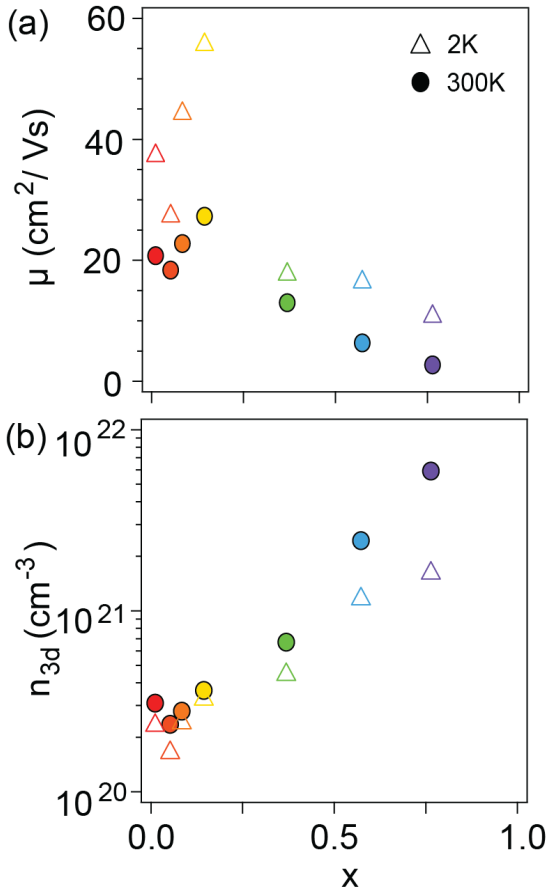

FIG. 3. **Transport measurements for films with varying Fe content.** (a) Mobility μ and (b) electron concentration n_{3d} as a function of excess Fe composition x at 300K and at 2K.

half-Heusler lattice [15].

We now discuss SQUID magnetometry measurements, focusing first on the samples with $x > 0.1$. These samples show nonlinear behavior in the magnetization (M) versus applied field (H) at room temperature (Fig. 4(a)), and the behavior is nearly independent of temperature in the range from 300K to 50K (Supplemental Fig. S-4b). These data suggest that for $x > 0.1$, the Curie temperature of the observed ferromagnetic ordering is much higher than 300K, consistent ferromagnetic Fe precipitates. In contrast, dilute magnetic doping in FeVSb and ferromagnetic proximity effects at Fe/FeVSb interfaces are expected to onset at lower temperatures and have a weaker magnetic response. For $x > 0.1$ the room temperature saturation magnetization M_{sat} increases linearly with x (Fig. 4(b)), also suggesting that the total magnetization is dominated by the local moment of precipitated Fe nanoparticles. Similar behavior is observed in Hall effect measurements, for which we observe nonlinearities that may be attributed to the anomalous Hall effect (Supplemental Fig. S-3).

The $x = 0.01$ sample also displays a weak $M(H)$ nonlinearity at room temperature, suggestive of ferromagnetic impurities, but has a slightly stronger temperature dependence (Supplemental Fig. S-4a). At this point, it is unclear whether the apparent room temperature ferromagnetism in this sample is due to Fe precipitates or due to other sources of nonstoichiometry (or point defects), since 1% is within the typical error bar for composition measurements.

To understand possible magnetism induced in the FeVSb, especially in the low x limit, we investigate the temperature-dependent magnetoresistance $\Delta\rho_{xx}(H)/\rho_{xx}(0)$. Unlike magnetometry, which detects the sum of all moments in the sample, we expect magnetoresistance to be dominated by the FeVSb matrix, since FeVSb forms a continuous conduction path. The Fe precipitates, in contrast, are disconnected. Fig. 5(a-c) shows the temperature dependence of the magnetoresistance for

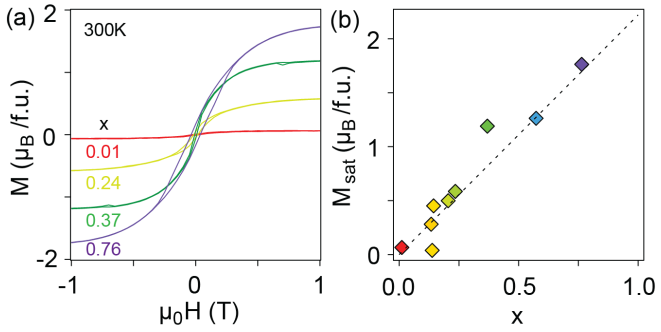

FIG. 4. **Magnetism from precipitated Fe nanoparticles, as measured by SQUID.** (a) Magnetization $M(H)$ for films with varying excess Fe composition. The diamagnetic contribution from the substrate has been subtracted. H was applied out of the sample plane ($H \parallel [001]$). (b) Saturation magnetization, M_{sat} as a function of x. The linear dependence of M_{sat} on X_{Fe} follows the Slater-Pauling curve for bcc Fe, as marked by the dotted line. Magnetization is expressed in units of Bohr magneton (μ_B) per formula unit (f.u.) of FeVSb.

samples with varying x. For $x = 0.01$, near stoichiometric condition, the magnetoresistance is negative and the magnetoresistance curve exhibits a broad zero field peak. We attribute the broad peak to localization from bound magnetic polarons [18] due to slight nonstoichiometry. Similar behavior has been observed for the half-Heusler compound CoTiSb [4, 19] and Mn-doped Ge [20, 21]. For $x = 0.05$ and 0.37 we observe butterfly shaped hysteresis at low temperature, ordering [4, 22].

We track the low temperature onset T_c^* of magnetic ordering by extracting the width of the magnetoresistance. We define the effective coercive field H_C^* as the field separation between the minima of the $\Delta\rho_{xx}(H)/\rho_{xx}(0)$ curves (supplement Fig. S-5) and the onset temperature T_c^* as the temperature at which H_C^* goes to zero. Fig. 5(d) tracks $H_C^*(T)$ for the same samples in Fig. 5(a-c). For $x = 0.05$, we find that the T_c^* is less than 5 K. One possible origin of this T_c^* is the onset of dilute ferromagnetism in the FeVSb semiconductor. For $x = 0.37$, which is above the solubility limit, we find $T_c^* \sim 20$ K. A possible origin of this T_c^* is the onset of proximity-induced ferromagnetism or superparamagnetism in the FeVSb, from the Fe/FeVSb interfaces. Alternatively, for both $T_c^* \sim 5$ K and ~ 2 K the magnetic onset may result from coupling between locally ferromagnetic Fe-rich FeVSb regions, as has been observed for carrier-mediated coupling between Mn-rich clusters in Mn_xGe_{1-x} films [20, 21] and superparamagnetic coupling between Fe-rich regions in $CoTi_xFe_{1-x}Sb$ films [4]. Further microstructure and magnetic measurements are required to fully understand the origin of the T_c^* in our $Fe_{1+x}VSb$ composites. Both T_c^*s are significantly smaller than the T_c for Fe precipitates (1043 K [17]).

III. CONCLUSION

In summary, we have demonstrated the MBE synthesis of epitaxial $Fe_{1+x}VSb$ films and provided an estimate for the solubility limit of Fe in FeVSb under these (non-equilibrium) growth conditions. Hysteresis in the low temperature magnetoresistance suggests dilute magnetic semiconducting behavior or proximity-induced ferromagnetism. For $x > 0.1$, epitaxial Fe precipitates form, embedded within the FeVSb semiconducting matrix. Two distinct sources of magnetism are identified for Fe: FeVSb nanocomposites: (1) ferromagetism of Fe nanoparticles detected in magnetometry and (2) proximity effect induced magnetism in FeVSb matrix or superparamagnetism detected in the magnetoresistance measurements. Our work provide a clean platform for the study of magnetic, nanocomposite Heusler systems. Further experiments are required to determine the solubility limit for excess Fe in FeVSb.

IV. ACKNOWLEDGMENTS

This work was supported by the CAREER program of the National Science Foundation (DMR-1752797) and by the SEED program of the Wisconsin Materials Research Science and Engineering Center, an NSF funded center (DMR-1720415). We gratefully acknowledge the use of X-ray diffraction and electron microscopy facilities supported by the NSF through the University of Wisconsin Materials Research Science and Engineering Center under Grant No. DMR-1720415. Electron microscopy characterization was supported by DOE (DE-FG02-08ER46547). We thank Professor Song Jin for the use of PPMS facilities. The Quantum Design MPMS3 magnetometer was supported by the UW Madison Department of Chemistry. We thank Greg Haugstad (Characterization Facility, University of Minnesota) for performing RBS measurements.

[1] D. Jung, H.-J. Koo, and M.-H. Whangbo, Journal of Molecular Structure: THEOCHEM **527**, 113 (2000).
[2] H. C. Kandpal, C. Felser, and R. Seshadri, Journal of Physics D: Applied Physics **39**, 776 (2006).
[3] J. Tobola, J. Pierre, S. Kaprzyk, R. Skolozdra, and M. Kouacou, Journal of Physics: Condensed Matter **10**, 1013 (1998).
[4] S. D. Harrington, A. D. Rice, T. Brown-Heft, B. Bonef, A. Sharan, A. P. McFadden, J. A. Logan, M. Pendharkar, M. M. Feldman, O. Mercan, et al., Physical Review Materials **2**, 014406 (2018).
[5] F. Casper, T. Graf, S. Chadov, B. Balke, and C. Felser, Semiconductor Science and Technology **27**, 063001 (2012).

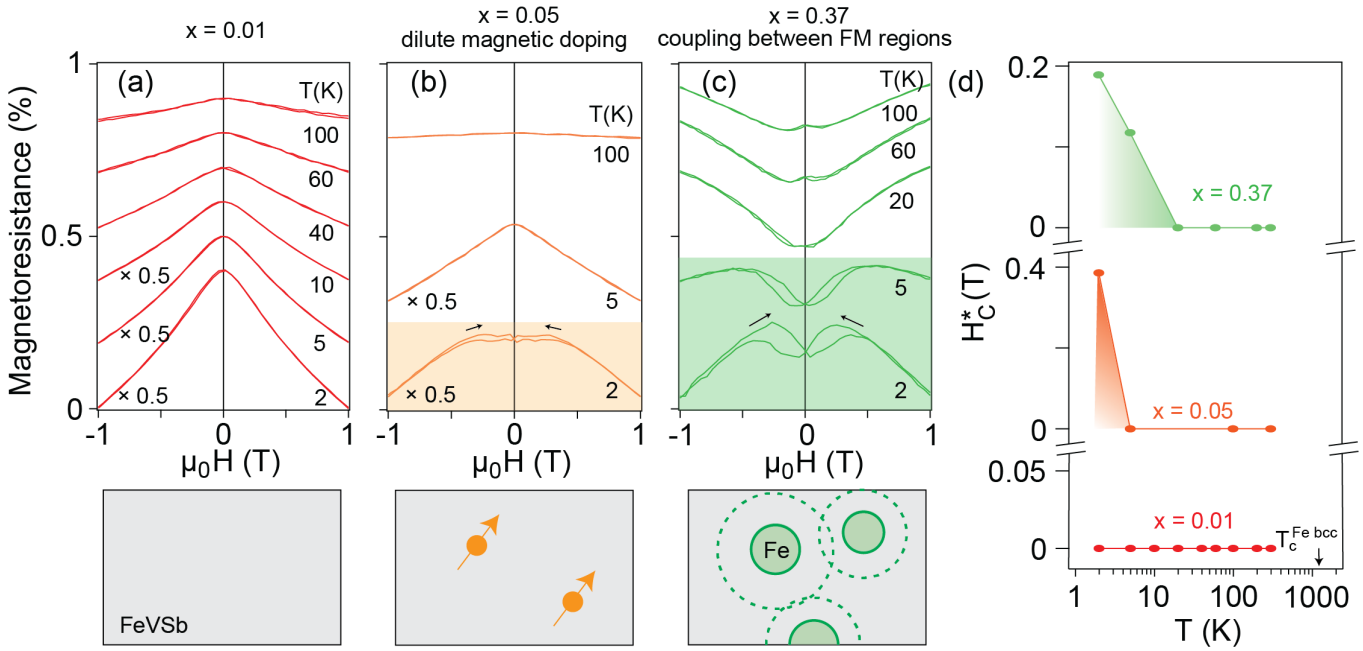

FIG. 5. **Dilute magnetism and ferromagnetic proximity effect in the FeVSb matrix.** (a-c) Magnetoresistance $[\rho_{xx}(H) - \rho_{xx}(0)]/\rho_{xx}(0)$ for $Fe_{1+x}VSb$ samples with $x = 0.01$, 0.05, and 0.37. (d) Width of the magnetoresistance hysteresis as a function of temperature. The T_c for bulk Fe is from Ref. [17].

[6] L. Wollmann, A. K. Nayak, S. S. Parkin, and C. Felser, Annual Review of Materials Research **47**, 247 (2017).
[7] D. Young, P. Khalifah, R. Cava, and A. Ramirez, Journal of Applied Physics **87**, 317 (2000).
[8] J. E. Douglas, C. S. Birkel, M.-S. Miao, C. J. Torbet, G. D. Stucky, T. M. Pollock, and R. Seshadri, Applied Physics Letters **101**, 183902 (2012).
[9] K. Vandaele, S. J. Watzman, B. Flebus, A. Prakash, Y. Zheng, S. R. Boona, and J. P. Heremans, Materials Today Physics **1**, 39 (2017).
[10] N. Tsujii, A. Nishide, J. Hayakawa, and T. Mori, Science advances **5**, eaat5935 (2019).
[11] J. Toboła and J. Pierre, Journal of Alloys and Compounds **296**, 243 (2000).
[12] V. V. Romaka, L. Romaka, Y. Stadnyk, V. Gvozdetskii, R. Gladyshevskii, N. Skryabina, N. Melnychenko, V. Hlukhyy, and T. Fässler, European Journal of Inorganic Chemistry **2012**, 2588 (2012).
[13] E. H. Shourov, R. Jacobs, W. A. Behn, Z. J. Krebs, C. Zhang, P. J. Strohbeen, D. Du, P. M. Voyles, V. W. Brar, D. D. Morgan, et al., Phys. Rev. Materials **4**, 073401 (2020).
[14] J. K. Kawasaki, A. Sharan, L. I. Johansson, M. Hjort, R. Timm, B. Thiagarajan, B. D. Schultz, A. Mikkelsen, A. Janotti, and C. J. Palmstrøm, Science Advances **4**, eaar5832 (2018).
[15] G. Y. Yonggang, X. Zhang, and A. Zunger, Physical Review B **95**, 085201 (2017).
[16] A. Rice, J. Kawasaki, N. Verma, D. Pennachio, B. Schultz, and C. Palmstrøm, Journal of Crystal Growth **467**, 71 (2017).
[17] N. Rosengaard and B. Johansson, Physical Review B **55**, 14975 (1997).
[18] D. Schmidt, A. Petukhov, M. Foygel, J. Ibbetson, and S. Allen, Physical review letters **82**, 823 (1999).
[19] J. K. Kawasaki, L. I. Johansson, B. D. Schultz, and C. J. Palmstrøm, Applied Physics Letters **104**, 022109 (2014).
[20] A. Li, J. Shen, J. Thompson, and H. Weitering, Applied Physics Letters **86**, 152507 (2005).
[21] A.-P. Li, J. Wendelken, J. Shen, L. C. Feldman, J. R. Thompson, and H. H. Weitering, Physical Review B **72**, 195205 (2005).
[22] M. Ziese, Reports on Progress in Physics **65**, 143 (2002).